Article

Supramolecular Chemistry of Halogens: Complementary Features of Inorganic (M–X) and Organic (C–X') Halogens Applied to M–X···X'–C Halogen Bond Formation

Fiorenzo Zordan, Lee Brammer, and Paul Sherwood

J. Am. Chem. Soc., **2005**, 127 (16), 5979-5989• DOI: 10.1021/ja0435182 • Publication Date (Web): 31 March 2005

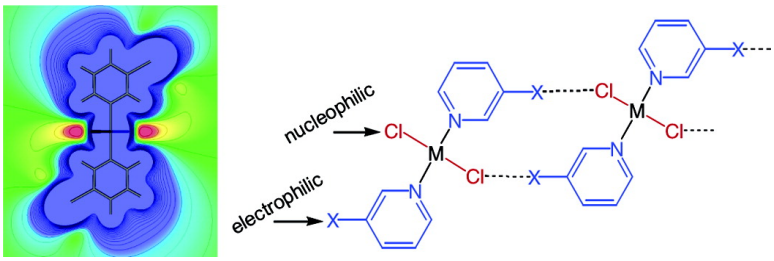

More About This Article

Additional resources and features associated with this article are available within the HTML version:

- Supporting Information
- Links to the 28 articles that cite this article, as of the time of this article download
- Access to high resolution figures
- Links to articles and content related to this article
- Copyright permission to reproduce figures and/or text from this article

View the Full Text HTML

J|A|C|S
ARTICLES
Published on Web 03/31/2005

Supramolecular Chemistry of Halogens: Complementary Features of Inorganic (M−X) and Organic (C−X′) Halogens Applied to M−X···X′−C Halogen Bond Formation

Fiorenzo Zordan,[†] Lee Brammer,*[,†] and Paul Sherwood[‡]

Contribution from the Department of Chemistry, University of Sheffield, Sheffield S3 7HF, U.K., and Computational Science and Engineering Department, CCLRC Daresbury Laboratory, Daresbury, Warrington WA4 4AD, U.K.

Received October 26, 2004; E-mail: lee.brammer@sheffield.ac.uk

Abstract: Electronic differences between inorganic (M−X) and organic (C−X) halogens in conjunction with the anisotropic charge distribution associated with terminal halogens have been exploited in supramolecular synthesis based upon intermolecular M−X···X′−C halogen bonds. The synthesis and crystal structures of a family of compounds *trans*-$[MCl_2(NC_5H_4X\text{-}3)_2]$ (M = Pd(II), Pt(II); X = F, Cl, Br, I; NC_5H_4X-3 = 3-halopyridine) are reported. With the exception of the fluoropyridine compounds, network structures propagated by M−Cl···X−C halogen bonds are adopted and involve all M−Cl and all C−X groups. M−Cl···X−C interactions show Cl···X separations shorter than van der Waals values, shorter distances being observed for heavier halogens (X). Geometries with near linear Cl···X−C angles (155−172°) and markedly bent M−Cl···X angles (92−137°) are consistently observed. DFT calculations on the model dimers $\{$*trans*-$[MCl_2(NH_3)(NC_5H_4X\text{-}3)]\}_2$ show association through M−Cl···X−C (X ≠ F) interactions with geometries similar to experimental values. DFT calculations of the electrostatic potential distributions for the compounds *trans*-$[PdCl_2(NC_5H_4X\text{-}3)_2]$ (X = F, Cl, Br, I) demonstrate the effectiveness of the strategy to activate C−X groups toward halogen bond formation by enhancing their electrophilicity, and explain the absence of M−Cl···F−C interactions. The M−Cl···X−C halogen bonds described here can be viewed unambiguously as nucleophile−electrophile interactions that involve an attractive electrostatic contribution. This contrasts with some types of halogen−halogen interactions previously described and suggests that M−Cl···X−C halogen bonds could provide a valuable new synthon for supramolecular chemists.

Introduction

Halogens have a ubiquitous presence in both inorganic and organic chemistry, serving as monodentate or bridging ligands for a wide variety of d-block, f-block, and main group metals as well being common substituents in a large number of organic compounds. Most frequently they lie at the periphery of molecules. The resultant steric accessibility has the potential to make halogenated compounds an attractive target for use in supramolecular chemistry and crystal engineering wherein the halogen atoms are directly involved in forming intermolecular interactions. Indeed interest in packing arrangements of halogenated compounds goes back many years to what Schmidt called the "chloro effect", wherein the presence of chloro substituents on aromatic compounds frequently resulted in stacking arrangements with a resultant short (ca. 4 Å) crystallographic axis.[1,2] Chloroaromatic compounds have also been intensely studied in the development of accurate anisotropic atom−atom potentials for organic crystal structure prediction.[3]

Some years ago Parthasarathy and colleagues examined the nature of groups forming short contacts with organic halogens (C−X) in the solid state and concluded that nucleophiles approach approximately along the C−X bond axis, while electrophiles approach the halogen in a roughly orthogonal direction.[4] They rationalized these observations in terms of nucleophile interactions with the C−X group LUMO (its σ^* orbital) and electrophile interactions with the C−X group HOMO, a predominantly p orbital-based lone pair (Scheme 1). However, the situation is not quite as simple as this orbital model alone suggests.

The interaction of nucleophiles with C−X groups has subsequently been studied in detail by Allen and co-workers,[5] who found a propensity in crystals for nitrogen and oxygen atoms to form short contacts with carbon-bound halogens (X = Cl, Br, I) at C−X···O/N angles approaching 180°, consistent with **I**. This is most pronounced for the heavier halogens. Significantly, neither short contacts nor an orientational preference is observed for interactions involving C−F groups.

[†] University of Sheffield.
[‡] CCLRC Daresbury Laboratory.

(1) (a) Green, B. S.; Schmidt, G. M. J. Israel Chemical Society annual meeting abstracts, **1971**, 197. See also the discussion in ref 2, chapter 6, and further references therein. (b) Cohen, M. D.; Schmidt G. M. J.; Sonntag, F. I. *J. Chem. Soc.* **1964**, 2000. (c) Schmidt, G. M. J. *J. Chem. Soc.* **1964**, 2014.
(2) Desiraju, G. R. *Crystal Engineering: The Design of Organic Solids*; Elsevier: Amsterdam, 1989.
(3) (a) Price, S. L.; Stone, A. J.; Lucas, J.; Rowland, R. S.; Thomleyt, A. E. *J. Am. Chem. Soc.* **1994**, *116*, 4910. (b) Day, G. M.; Price, S. L. *J. Am. Chem. Soc.* **2003**, *125*, 16434.
(4) Ramasubbu, N.; Parthasarathy, R.; Murray-Rust, P. *J. Am. Chem. Soc.* **1986**, *108*, 4308.
(5) Lommerse, J. P. M.; Stone, A. J.; Taylor, R.; Allen, F. H. *J. Am. Chem. Soc.* **1996**, *118*, 3108.

Scheme 1. Typical Interaction Geometries for Nucleophiles (Nu) I and Electrophiles (El) II with Halocarbons (C−X) Rationalized in Terms of HOMO−LUMO Interactions[4]

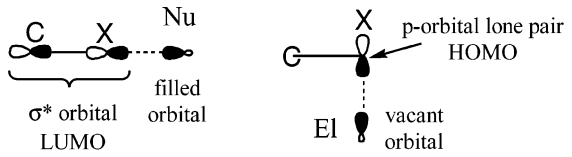

I II

Scheme 2. Anisotropic Exchange Repulsion and Electrostatic Interactions for Interactions of C−X Groups with Nucleophiles[5]

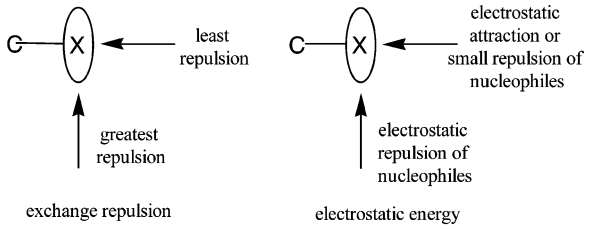

III IV

Complementary ab initio calculations using intermolecular perturbation theory (IMPT) methods applied to a series of model systems showed that approximately linear C−Cl···O/N interactions provide the lowest energy configuration. In all cases this geometry is facilitated by an anisotropic exchange repulsion contribution to the energy, which is at a minimum along the C−Cl bond axis (Scheme 2, **III**). This is the origin of the proposed anisotropic van der Waals radius for halogens[6] and provides an explanation for the packing of simple chlorohydrocarbons via C−Cl···Cl−C short contacts,[3a] though other opinions have been expressed on this matter.[7] For the $CH_3Cl\cdots O{=}CH_2$ model dimer[5] the anisotropic electrostatic potential around the halogen (see, Figure 1a) means that the electrostatic interaction energy term is repulsive, but least repulsive for a linear C−Cl···O geometry (Scheme 2, **IV**), thereby reinforcing the geometry favored by the exchange repulsive term. In fact, in this example the overall interaction is repulsive as the attractive charge transfer, polarization, and dispersion terms are small in magnitude. However, analogous calculations for the $NC{-}C{\equiv}C{-}Cl\cdots O{=}CH_2$ model dimer show that while the anisotropic repulsion and electrostatic terms still favor the linear C−Cl···O geometry, the electron-withdrawing alkyne and nitrile groups "activate" the C−Cl group, resulting in an *attractive* electrostatic term, which combined with the attractive second-order energy terms leads to attractive overall C−Cl···O interaction.

We have previously noted the marked difference in hydrogen bond acceptor capability between organic (C−X) and inorganic (M−X) halogens that arises primarily from the far greater polarity of the M−X bond.[8] These studies confirm the preference of *electrophiles*, in this case hydrogen bond donors (e.g., N−H), to interact with C−X groups with a geometry resembling **II**.[8a] However, such interactions are weak not only for hydrogen bond donors but where metal ions serve as the electrophiles. In contrast, when bound to metal centers, halogens become much stronger hydrogen bond acceptors[8] and analogously form stronger secondary interactions with other metal centers. This contrast is illustrated by comparison of the electrostatic potential associated with inorganic halogens (M−X) and with organic halogen counterparts (C−X) shown in Figure 1. While both are similarly anisotropic, the magnitude of the negative potential is far greater for the inorganic halogens. Nevertheless, the anisotropic potential provides the basis for directional interactions that can be exploited in supramolecular assembly.

In the context of supramolecular synthesis, the properties of halogens in organic molecules as electrophiles have been well established for the heavier halogens.[9] The resulting interactions can be strong enough to influence the aggregation of organic molecules in gas, liquid, and solid phase, and the term "halogen bonding" has been introduced in order to establish an evident analogy with hydrogen bonding.[10] In addition, the hydrogen bond acceptor properties of halogens bound to transition metals have led to the combination of halometalate ions, MX_m^{n-} (M = metal, X = Cl, Br), with cationic organic building blocks to yield new hybrid ionic hydrogen-bonded materials, based on supramolecular synthons such as N−H···X−M, N−H···X_2M, and N−H···X_3M.[11]

It is the exploitation of these differences between organic and inorganic halogens that we seek to explore in developing a new class of supramolecular synthons (M−X···X′−C) for applications in supramolecular chemistry and crystal engineering. Our strategy focuses on facilitating interactions between inorganic halogens and suitably "activated" organic halogens wherein an attractive electrostatic component may maximize the efficacy of the anticipated directional interactions. Activation of the organic halogen has been pursued through use of halopyridines wherein the ring nitrogen atom exerts an electron-withdrawing effect.[12] The C−X groups can then be further activated either by protonation of the pyridine nitrogen or its coordination to a metal center (Scheme 3) or, as demonstrated by Resnati and co-workers, by pyridine nitrogen methylation.[13] The first approach (Scheme 3, i) has recently led to the synthesis of hybrid *ionic* materials in which organic cations and halometalate anions are linked via charge-assisted M−X···X′−C halogen bond synthons (X = Cl, Br, I; X′ = Cl, Br; M = Co(II), Cu(II)).[14] Here we pursue the second approach (Scheme 3, ii) and present the synthesis and characterization of a series of molecular crystals of general formula *trans*-$MCl_2(NC_5H_4X\text{-}3)_2$ (M = Pd(II), Pt(II); X = F, Cl, Br, I; NC_5H_4X-3 = 3-halopyridine) designed in order to establish the applicability of the M−Cl···X−C interaction as an effective Lewis acid−Lewis base pair synthon for supramolecular construction from neutral

(6) (a) Nyburg, S. C.; Wong-Ng, W. *Proc. R. Soc. London* **1979**, *A367*, 29. (b) Nyburg, S. C. *Acta Crystallogr.* **1979**, *A35*, 641. (c) Nyburg, S. C.; Faerman, C. H. *Acta Crystallogr.* **1985**, *B41*, 274.
(7) Desiraju, G. R.; Parthasarathy, R. *J. Am. Chem. Soc.* **1989**, *111*, 8725.
(8) (a) Brammer, L.; Bruton, E. A.; Sherwood, P. *Cryst. Growth Des.* **2001**, *1*, 277. (b) Aullón, G.; Bellamy, D.; Brammer, L.; Bruton, E. A.; Orpen, A. G. *Chem. Commun.* **1998**, 653.
(9) (a) Corradi, E.; Meille, S. V.; Messina, M. T.; Metrangolo, P. Resnati, G. *Angew. Chem., Int. Ed.* **2000**, *39*, 1782. (b) Metrangolo, P.; Resnati, G. *Chem. Eur. J.* **2001**, *7*, 2511. (c) Bailey Walsh, R.; Padgett, C. W.; Metrangolo, P.; Resnati, G.; Hanks, T. W.; Pennington, W. T. *Cryst. Growth Des.* **2001**, *1*, 165. (d) Thallapally, P. K.; Desiraju, G. R.; Bagieu-Beucher, M.; Masse, R.; Bourgogne, C.; Nicoud, J.-F. *Chem. Commun.* **2002**, 1052.
(10) Legon, A. C. *Angew. Chem., Int. Ed.* **1999**, *38*, 2687.
(11) (a) Brammer, L.; Swearingen, J. K.; Bruton, E. A.; Sherwood, P. *Proc. Nat. Acad. Sci., U.S.A.* **2002**, *99*, 4956. (b) Mareque Rivas, J. C.; Brammer, L. *Inorg. Chem.* **1998**, *37*, 4756. (c) Lewis, G. R.; Orpen, A. G. *J. Chem. Soc., Chem. Commun.* **1998**, 1873.
(12) Janiak, C. *J. Chem. Soc., Dalton Trans.* **2000**, 3885.
(13) Logothetis, T. A.; Meyer, F.; Metrangolo, P.; Pilati, T.; Resnati, G. *New J. Chem.* **2004**, *28*, 760.
(14) (a) Brammer, L.; Mínguez Espallargas, G.; Adams, H. *CrystEngComm* **2003**, *5*, 343. (b) Willett, R. D.; Awwadi, F.; Butcher, R.; Haddad, S.; Twamley, B. *Cryst. Growth Des.* **2003**, *3*, 301. (c) Freytag, M.; Jones, P. G. *Chem. Commun.* **2000**, 277.

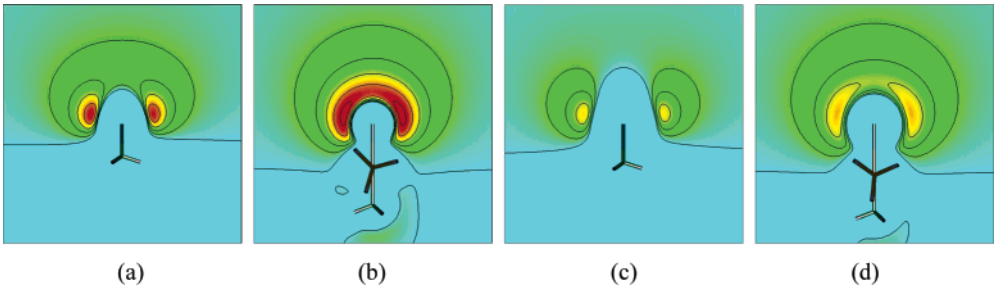

Figure 1. Negative electrostatic potential distributions for (a) CH_3Cl, (b) *trans*-$PdCl(Me)(PH_3)_2$, (c) CH_3I, and (d) *trans*-$PdI(Me)(PH_3)_2$. Contour levels are at 4 kcal/mol for the organic halogens (C−X) in (a) and (c) and at 10 kcal/mol for the inorganic halogens (M−X) in (b) and (d). (Figure adapted from ref 8a with permission of the American Chemical Society.)

Scheme 3. Approaches to "Activating" Organic Halogens (C−X) toward Interactions with Nucleophiles, Leading to Applications in Which M−Cl···X−C Halogen Bonds Can Be Used for Supramolecular Assembly

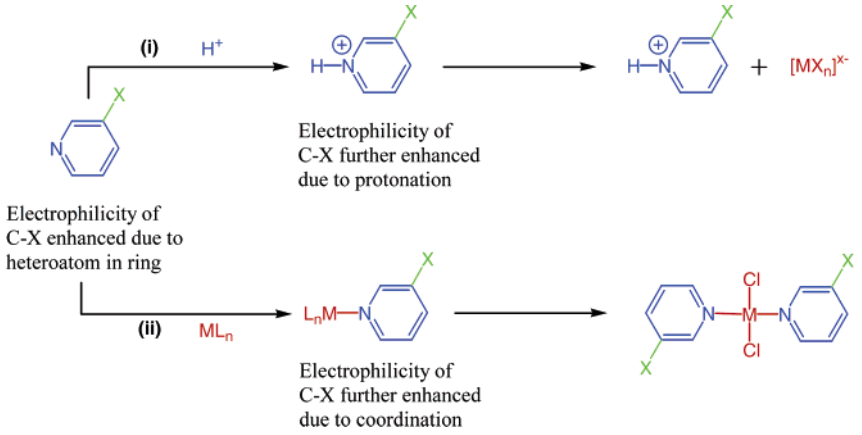

building blocks.[15] The synthetic studies are supported by DFT calculations on model systems and ab initio electrostatic potential calculations on the *trans*-$PdCl_2(NC_5H_4X\text{-}3)_2$ series of compounds. The resulting crystal structures provide compelling evidence for the efficacy of the M−Cl···X−C synthon (X ≠ F), which clearly defines extended 1D or 2D motifs in all cases.

Experimental Section

General Procedures. All reagents (purchased from Aldrich or Lancaster) and solvents were used as received. Single crystals of all compounds were prepared by one of methods A−C. An alternative method (D) was employed to prepare some samples as powders. Elemental analyses were conducted by the Elemental Analysis Service, Department of Chemistry, University of Sheffield. Powder diffraction data were obtained using Cu Kα radiation on a Bruker D8 diffractometer in reflection mode. Thermal gravimetric analyses of **1** and **5**·MeOH were conducted using a Perkin-Elmer Series 7 TGA instrument at a scan speed of 1 °C/min.

General Procedures for Crystal Synthesis. Method A. Crystals were obtained by diffusion between immiscible layers at room temperature (20 °C). In small vials an acidified aqueous phase containing the metal salt was layered upon a CH_2Cl_2 phase containing the halopyridine. All the vials were sealed with a plastic lid during crystal growth.

Method B. This method is a variant of method A in which a third phase (toluene) was layered between the aqueous phase containing the metal salt and an acidified MeOH phase containing the halopyridine to reduce the rate of diffusion and thus mixing of the two components.

Method C. Crystals were obtained at room temperature (20 °C) by a method based on slow diffusion in U-shaped tubes (internal diameter 5 mm). Methanolic solutions containing the metal salt and the halopyridine, respectively, were prepared, the latter acidified using HCl. The two solutions were layered in separate arms of the U-tube above a basal layer of CH_2Cl_2. Both arms of the U-tube were then sealed with Parafilm.

Method D (for synthesis of crystalline powders of compounds 5−8). Typically 40 mg of Na_2PdCl_4 was dissolved in 2 mL of MeOH/CH_2Cl_2 (1:1) (solution I), and a stoichiometric amount of halopyridine was dissolved in 2 mL of MeOH previously acidified using 30 mg of HCl (37% aqueous) (solution II). The two solutions I and II were kept separated in a vial-in-vial system, and enough MeOH (ca. 20 mL) was very slowly added into the larger vial in order to put the solutions in contact. The process of diffusion was generally faster than that observed with the U-tubes (method C), and within 2 weeks all the samples prepared yielded very thin yellow needle-shaped crystals (same morphology as those obtained from the U-tubes), not suitable for analysis as single crystals but suitable for elemental analysis and powder diffraction.

Synthesis of *trans*-$[PtCl_2(NC_5H_4F\text{-}3)_2]$ (1). K_2PtCl_4 (30 mg, 0.072 mmol) in acidic aqueous solution (pH ≈ 4, 2 mL) was layered on 3-fluoropyridine (15 mg, 0.154 mmol) in CH_2Cl_2 (2 mL) using method A. Yellow prismatic crystals of **1** (24.6 mg, yield 74.1%) resulted after 4 weeks. Anal. Calc: C, 26.08; H, 1.73; N, 6.08. Found: C, 25.91; H, 1.71; N, 5.87. The powder diffraction pattern (bulk sample) was consistent with the pattern calculated from single-crystal data.

Synthesis of *trans*-$[PtCl_2(NC_5H_4Cl\text{-}3)_2]$ (2). K_2PtCl_4 (30 mg, 0.072 mmol) in acidic aqueous solution (pH ≈ 4, 2 mL) was layered on 3-chloropyridine (16 mg, 0.140 mmol) in CH_2Cl_2 (2 mL) using method A. Yellow prismatic crystals of **2** (34.8 mg, yield 98%) resulted after 1 week. Anal. Calc: C, 24.34; H, 1.62; N, 5.68. Found: C, 24.29; H, 1.58; N, 5.53. The powder diffraction pattern (bulk sample) was consistent with the pattern calculated from single-crystal data.

Synthesis of *trans*-$[PtCl_2(NC_5H_4Br\text{-}3)_2]$ (3a). K_2PtCl_4 (30 mg, 0.072 mmol) in acidic aqueous solution (pH ≈ 4, 4 mL) and 3-bromopyridine (22 mg, 0.140 mmol) in CH_2Cl_2 solution (6 mL) were prepared. The

(15) Pennington has also reported neutral Cd−I···I−I interactions: Bailey, R. D.; Hook, L. L.; Pennington, W. T. *Chem. Commun.* **1998**, 1181.

aqueous solution (2 mL) was layered on the CH_2Cl_2 solution (2 mL) using method A. Yellow needle-shaped crystals of **3a** (40.8 mg, yield 97.3%) resulted after 4 weeks. Anal. Calc: C, 20.62; H, 1.37; N, 4.81. Found: C, 20.44; H, 1.43; N, 4.67. The powder diffraction pattern (bulk sample) was consistent with the pattern calculated from single-crystal data.

Synthesis of *trans*-[$PtCl_2(NC_5H_4Br\text{-}3)_2$] (3b). 3-Bromopyridine (40 mg, 0.253 mmol) in MeOH (2 mL), previously acidified using 30 mg of HCl (37% aqueous), was layered on toluene (5 mL), which in turn had been layered upon K_2PtCl_4 (10 mg, 0.024 mmol) in H_2O (2 mL). This procedure follows method B. Thin yellow needle-shaped crystals of **3b** were first observed after 2 weeks. Thicker crystals were harvested after a further 5 weeks (12.3 mg, yield 88.0%). Anal. Calc: C, 20.62; H, 1.37; N, 4.81. Found: C, 20.49; H, 1.39; N, 4.57. The powder diffraction pattern (bulk sample) did not indicate a homogeneous phase but could not simply be analyzed as a mixture of **3a** and **3b**.

Synthesis of *trans*-[$PtCl_2(NC_5H_4I\text{-}3)_2$] (4). K_2PtCl_4 (30 mg, 0.072 mmol) in acidic aqueous solution (pH ≈ 4, 2 mL) was layered on 3-iodopyridine (30 mg, 0.146 mmol) in CH_2Cl_2 (2 mL). Yellow laminar crystals of **4** (46.9 mg, yield 96.3%) resulted after 1 week. Anal. Calc: C, 17.75; H, 1.18; N, 4.14. Found: C, 17.48; H, 1.17; N, 3.80. The powder diffraction pattern (bulk sample) was consistent with the pattern calculated from single-crystal data.

Synthesis of *trans*-[$PdCl_2(NC_5H_4F\text{-}3)_2$]·MeOH (5·MeOH). Na_2PdCl_4 (25 mg, 0.084 mmol) was dissolved in MeOH (2 mL) (solution A), and 3-fluoropyridine (17 mg, 0.175 mmol), to which 20 mg of HCl (37% aqueous solution) had been previously added, was diluted using MeOH (2 mL) (solution B). Following method C, solution A (1 mL) and solution B (1 mL) were respectively layered in separate arms of a U-tube above CH_2Cl_2 (2 mL). Thick yellow needle-shaped crystals of **5**·MeOH (<1 mg) resulted after 16 weeks. A powder sample of **5**·MeOH was prepared according to method D (yield 54%). The powder diffraction pattern (bulk sample) was consistent with the pattern calculated from single-crystal data. Mass loss during combustion analysis prevented accurate determination of composition by this method. TGA analysis illustrates the problem in that a gradual loss of mass occurs with an onset around 100 °C, culminating in a total of 70% mass loss by 275 °C. This contrasts with the unsolvated Pt analogue (**1**), which is thermally stable up to 225 °C and then undergoes a sharp loss of mass (ca. 25%) upon further heating.

Synthesis of *trans*-[$PdCl_2(NC_5H_4Cl\text{-}3)_2$] (6). Na_2PdCl_4 (10 mg, 0.034 mmol) was dissolved in MeOH (10 mL) (solution A), and 3-chloropyridine (20 mg, 0.176 mmol), to which 60 mg of HCl (37% aqueous solution) had been previously added, was diluted using MeOH (2 mL) (solution B). Following method C, solution A (1 mL) and solution B (1 mL) were respectively layered in separate arms of a U-tube above CH_2Cl_2 (2 mL). Thick yellow needle-shaped crystals of **6** (<1 mg) resulted after 8 weeks. A powder sample of **6** was prepared according to method D (yield 71.6%). Anal. Calc: C, 29.68; H, 1.97; N, 6.92. Found: C, 29.17; H, 1.84; N, 6.52. The powder diffraction pattern (bulk sample) was consistent with the pattern calculated from single-crystal data.

Synthesis of *trans*-[$PdCl_2(NC_5H_4Br\text{-}3)_2$] (7). Na_2PdCl_4 (25 mg, 0.084 mmol) was dissolved in MeOH (2 mL) (solution A), and 3-bromopyridine (25 mg, 0.158 mmol), to which 20 mg of HCl (37% aqueous solution) had been previously added, was diluted using MeOH (2 mL) (solution B). Following method C, solution A (1 mL) and solution B (1 mL) were respectively layered in separate arms of a U-tube above CH_2Cl_2 (2 mL). Thick yellow needle-shaped crystals of **7** (ca. 2 mg) resulted after 3 weeks. A powder sample of **7** was prepared according to method D (yield 46.2%). Anal. Calc: C, 24.33; H, 1.62; N, 5.68. Found: C, 24.27; H, 1.54; N, 5.39. The powder diffraction pattern (bulk sample) was consistent with the pattern calculated from single-crystal data.

Synthesis of *trans*-[$PdCl_2(NC_5H_4I\text{-}3)_2$] (8). Na_2PdCl_4 (25 mg, 0.084 mmol) was dissolved in MeOH (2 mL) (solution A), and 3-iodopyridine (35 mg, 0.170 mmol), to which 20 mg of HCl (37% aqueous solution) had been previously added, was diluted using MeOH (2 mL) (solution B). Following method C, solution A (1 mL) and solution B (1 mL) were respectively layered in separate arms of a U-tube above CH_2Cl_2 (2 mL). Thin yellow needle-shaped crystals of **8** were observed after 4 weeks. Thicker crystals (ca. 2 mg) were harvested after a further 4 weeks. A powder sample of **8** was prepared according to method D (yield 39.3%). Anal. Calc: C, 20.43; H, 1.36; N, 4.76. Found: C, 20.41; H, 1.32; N, 4.60. The powder diffraction pattern (bulk sample) was consistent with the pattern calculated from single-crystal data.

Crystallography. X-ray data were collected on a Bruker SMART 1000 diffractometer using Mo Kα radiation. Crystal structures were solved and refined against all F^2 values using the SHELXTL suite of programs.[16] A summary of the data collection and structure refinement information is provided in Table 1. Data were corrected for absorption using empirical methods (SADABS) based upon symmetry-equivalent reflections combined with measurements at different azimuthal angles.[17] Non-hydrogen atoms were refined anisotropically. Hydrogen atoms were placed in calculated positions, refined using idealized geometries (riding model), and assigned fixed isotropic displacement parameters. For **5**·MeOH, the methanol molecule is disordered between two positions related by a center of inversion, to each of which 50% occupancy was assigned.

Theoretical Calculations. Geometry optimizations for the four *trans*-$PdCl_2(NH_3)(NC_5H_4X\text{-}3)$ model complexes (X = F, Cl, Br, I) and their putative dimers were conducted using the GAMESS-UK[18] package, employing the B3LYP DFT functional.[19] The basis set and pseudopotentials used were LANL2DZ(dp);[20] for the lighter elements C, H, N, and F this was an all-electron Dunning DZP quality basis[21] and for Cl, Br, I, and Pd the effective core potentials (ECPs) of Hay and Wadt[22] were used, and the associated basis sets were augmented with diffuse and polarization function.[23] The optimization for the dimer $\{PdCl_2(NH_3)(NC_5H_4I)\}_2$ was initiated using a geometry resembling that observed in the crystal structure of compound **8**. Subsequent dimer optimizations were initiated from the same geometry after replacing the iodine atom with bromine, chlorine, and fluorine, respectively.

Electrostatic potentials for the $PdCl_2(NC_5H_4X\text{-}3)_2$ complexes (X = F, Cl, Br, I) were calculated at the B3LYP level using the GAMESS-UK[18] package, employing the effective core potentials (ECPs) of Hay and Wadt,[20,22] the LANL2DZ(dp)[20,23] basis set for Pd, and the Sadlej pVTZ (polarized valence triple-ζ) basis sets[20,24] on all

(16) *SHELXTL* 5.1; Bruker Analytical X-Ray Instruments, Inc., 1998.
(17) (a) Sheldrick, G. M. *SADABS*, Empirical absorption correction program; University of Göttingen, 1995, based upon the method of Blessing.[17b] (b) Blessing, R. H. *Acta Crystallogr.* **1995**, *A51*, 33.
(18) GAMESS-UK is a package of ab initio programs written by Guest, M. F.; van Lenthe, J. H.; Kendrick, J.; Schoffel, K.; Sherwood, P. with contributions from Amos, R. D.; Buenker, R. J.; van Dam, H. J. J.; Dupuis, M.; Handy, N. C.; Hillier, I. H.; Knowles, P. J.; Bonacic-Koutecky, V.; von Niessen, W.; Harrison, R. J.; Rendell, A. P.; Saunders: V. R.; Stone, A. J.; de Vries, A. H. The package is derived from the original GAMESS code due to Dupuis, M.; Spangler, D.; Wendoloski, J. NRCC Software Catalog, Vol. 1, Program No. QG01 (GAMESS), 1980.
(19) (a) Stephens, P. J.; Devlin, F. J.; Chabalowski, C. F.; Frisch, M. J. *J. Phys. Chem.* **1994**, *98*, 11623, and references therein. (b) *GAMESS-UK* uses the VWN 3 (RPA-type) parametrization; for details on this issue see: Hertwig, R. H.; Koch, W. *Chem. Phys. Lett.* **1997**, *268*, 345.
(20) All basis sets and ECP data were obtained from the Extensible Computational Chemistry Environment Basis Set Database, Version 02/25/04, as developed and distributed by the Molecular Science Computing Facility, Environmental and Molecular Sciences Laboratory, which is part of the Pacific Northwest Laboratory, P.O. Box 999, Richland, WA 99352, and funded by the U.S. Department of Energy. The Pacific Northwest Laboratory is a multiprogram laboratory operated by Battelle Memorial Institute for the U.S. Department of Energy under contract DE-AC06-76RLO 1830. Contact David Feller or Karen Schuchardt for further information.
(21) Dunning, T. H., Jr.; Hay, P. J. In *Methods of Electronic Structure Theory*, Vol. 2; Schaefer, H. F., III. Ed.; Plenum Press: New York, 1977.
(22) (a) Hay, P. J.; Wadt, W. R. *J. Chem. Phys.* **1985**, *82*, 270. (b) Hay, P. J.; Wadt, W. R. *J. Chem. Phys.* **1985**, *82*, 284. (c) Hay, P. J.; Wadt, W. R. *J. Chem. Phys.* **1985**, *82*, 299.
(23) Check, C. E.; Faust, T. O.; Bailey, J. M.; Wright, B. J.; Gilbert, T. M.; Sunderlin, L. S. *J. Phys. Chem. A* **2001**, *105*, 8111.
(24) Sadlej, A. J. *Theor. Chim. Acta* **1992,** *81*, 45, and references therein.

Table 1. Data Collection, Structure Solution, and Refinement Parameters for **1**−**8**

	1	**2**	**3a**	**3b**	**4**	**5**·MeOH	**6**	**7**	**8**
cryst color	yellow	yellow	yellow	yellow	yellow	yellow	yellow	yellow	yellow
cryst size (mm)	0.30 × 0.19 × 0.16	0.29 × 0.15 × 0.15	0.40 × 0.12 × 0.05	0.21 × 0.14 × 0.05	0.22 × 0.10 × 0.08	0.40 × 0.15 × 0.06	0.45 × 0.05 × 0.04	0.40 × 0.18 × 0.13	0.23 × 0.12 × 0.07
cryst syst	triclinic	triclinic	triclinic	triclinic	monoclinic	monoclinic	monoclinic	monoclinic	triclinic
space group, *Z*	$P\bar{1}$, 1	$P\bar{1}$, 1	$P\bar{1}$, 2	$P\bar{1}$, 1	*C*2/*c*, 4	$P2_1/c$, 2	$P2_1/c$, 2	$P2_1/c$, 2	$P\bar{1}$, 1
a (Å)	6.9562(4)	5.5441(7)	3.9786(11)	3.9673(7)	25.414(5)	3.8484(16)	3.911(3)	3.9496(7)	4.1501(6)
b (Å)	7.0192(4)	7.1432(9)	12.337(3)	8.3332(15)	4.2034(9)	11.719(5)	13.721(12)	13.924(2)	8.4147(11)
c (Å)	7.6303(4)	8.6648(11)	13.624(4)	10.1785(17)	16.357(3)	15.637(7)	12.029(10)	12.034(2)	10.1870(13)
α (deg)	64.148(3)	71.147(2)	90.462(4)	90.874(3)	90	90	90	90	90.787(2)
β (deg)	63.131(3)	79.634(2)	96.487(4)	97.659(3)	126.464(3)	96.578(7)	94.98(2)	93.529(3)	96.369(2)
γ (deg)	81.167(4)	85.992(2)	97.049(5)	101.560(3)	90	90	90	90	101.532(2)
V (Å^3)	298.64(3)	319.41(7)	659.4(3)	326.7(1)	1405.3(5)	700.6(5)	643.1(10)	660.6(2)	346.2(1)
density (Mg/m^3)	2.559	2.563	2.931	2.958	3.195	1.894	2.088	2.480	2.817
temperature (K)	150	150	150	150	150	150	150	150	150
μ(Mo Kα) (mm^{-1})	12.195	11.794	17.081	17.273	14.737	1.719	2.249	7.834	6.163
θ range (deg)	3.29 to 27.92	2.52 to 27.88	3.00 to 28.17	2.495 to 29.80	2.495 to 30.0	2.18 to 27.86	2.26 to 28.03	2.24 to 27.54	2.47 to 27.65
reflns collected	4858	3699	6337	3962	8029	6653	7248	7200	3950
indepndnt reflns, *n*, (R_{int})	1291 (0.0294)	1501 (0.0257)	2324 (0.1114)	1744 (0.0552)	1996 (0.0741)	1579 (0.0366)	1503 (0.1742)	1496 (0.0398)	1562 (0.0331)
reflns used in refinement	1291	1501	2324	1744	1996	1579	1503	1496	1562
L. S. params (p)	79	79	157	79	79	87	79	79	79
R1(F)^a, $I > 2.0\sigma(I)$	0.0145	0.0191	0.0538	0.0425	0.0391	0.0389	0.0672	0.0293	0.0260
wR2(F^2)^a, all data	0.0361	0.0480	0.1289	0.1009	0.0903	0.1116	0.1597	0.0771	0.0651
$S(F^2)^a$, all data	1.105	1.086	1.017	0.991	1.002	1.113	0.907	1.029	1.034

^{a} $R1(F) = \sum(|F_o| - |F_c|)/\sum|F_o|$; $wR2(F^2) = [\sum w(F_o^2 - F_c^2)^2/\sum wF_o^4]^{1/2}$; $S(F^2) = [\sum w(F_o^2 - F_c^2)^2/(n-p)]^{1/2}$.

other atoms. Molecular geometries were based upon those in the crystal structures of the corresponding molecules and the platinum analogues. Average values for intra-ring distances and angles were used to give the symmetrized ring geometries for all four compounds (see Supporting Information). An average C−N−Pd−Cl torsion angle of 55° was used for all calculations (cf. experimental values of 50−65°).

Results

Reaction of K_2PtCl_4 or Na_2PdCl_4 with the appropriate 3-halopyridine (NC_5H_4X-3) under acidic conditions permitted preparation of the entire series of compounds *trans*-[MCl_2-(NC_5H_4X-3)$_2$] (M = Pt, Pd; X = F, Cl, Br, I). Initial trials using direct mixing of miscible solutions of the two reactants yielded microcrystalline powders within minutes for the platinum systems and within seconds for the palladium analogues. Thus, slow mixing of solutions of the two reactants via immiscible phases (method A) was necessary to prepare crystals of the platinum compounds that were of suitable size for single-crystal X-ray diffraction studies. Method C, using the U-tubes, permitted the slowest mixing and proved necessary to prepare crystals of the palladium compounds. Compounds **1**−**8** were characterized by low-temperature X-ray crystallography, with two polymorphs being obtained for compound **3** under different synthetic conditions. All compounds crystallize such that the *trans*-[MCl_2(NC_5H_4X-3)$_2$] molecules adopt a crystallographically imposed centrosymmetric conformation. All compounds except **5**·MeOH gave satisfactory elemental analyses. With the exception of polymorph **3b**, powder diffraction studies confirmed the presence of a single phase consistent with the single-crystal structure determination for all compounds.

In all cases except that of the fluoropyridine systems, the crystal structure contains a network of molecules linked via M−Cl···X−C interactions. Two network types were found, namely, 1D tapes in which each molecule is linked to two neighbors via pairs of M−Cl···X−C interactions and 2D layers in which each molecule is linked to four neighbors via individual M−Cl···X−C interactions.

Tape Structures of *trans*-[$PtCl_2(NC_5H_4Cl$-3$)_2$] (2), *trans*-[$PtCl_2(NC_5H_4Br$-3$)_2$] (3b), and *trans*-[$PdCl_2(NC_5H_4I$-3$)_2$] (8). The structures of **2** and **8** and the polymorph **3b** comprise 1D tape motifs propagated along the *c*-axis in which neighboring molecules are centrosymmetrically linked via a pair of M−Cl···X−C interactions (**2**, X = Cl, M = Pt; **3b**, X = Br, M = Pt; **8**, X = I, M = Pd), as shown in Figures 2 and 3. In all cases these are the only halogen−halogen interactions in the structure. **3b** and **8** are isostructural, as is evident from unit cell parameters.

In **2** the Pt−Cl···Cl−C interaction has a Cl···Cl separation slightly shorter than the sum of the van der Waals radii of the two chlorine atoms and exhibits a large obtuse angle at the organic chloride, but a much smaller angle at the metal-bound chloride [(Pt)Cl···Cl(C) 3.443(1) Å, Pt−Cl···Cl 92.69(3)°, C−Cl···Cl 155.9(1)°]. The halogen-bonded ribbons further aggregate in the three-dimensional structure via C−H···Cl−Pt hydrogen bonds [(Pt)Cl···H(C) 2.864 Å, C−H···Cl 128.0°, Pt−Cl···H 115.1° and (Pt)Cl···H(C) 2.866 Å, C−H···Cl 131.0°, Pt−Cl···H 76.4°] and via offset stacking interactions of *centrosymmetrically* related halopyridine rings (Table 2 and Figure 12a, vide infra). Evidence for the supporting role of pairs of C−H···Cl−C interactions is also of note [(C)H···Cl(C) 2.759 Å, C−H···Cl 163.9°, C−Cl···H = 111.8° and (C)H···Cl(C) 2.894 Å, C−H···Cl 132.1°, C−Cl···H = 118.4°]. The shorter

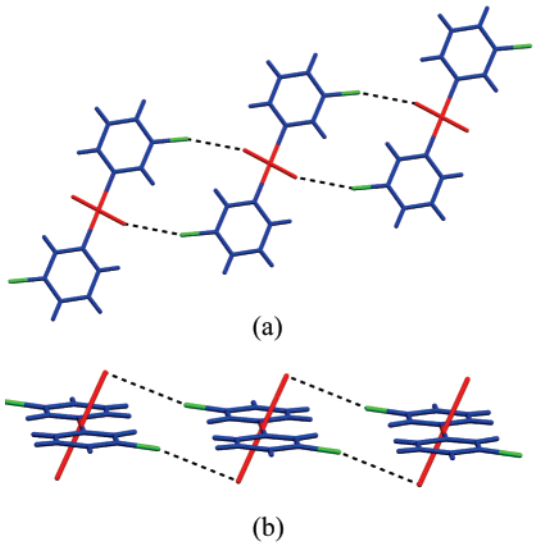

Figure 2. Views of **2** showing the tape network propagated via Pt−Cl···Cl−C interactions. Metal and chloride ligands are shown in red, organic halogens in green, and all other atoms (N, C, H) in blue.

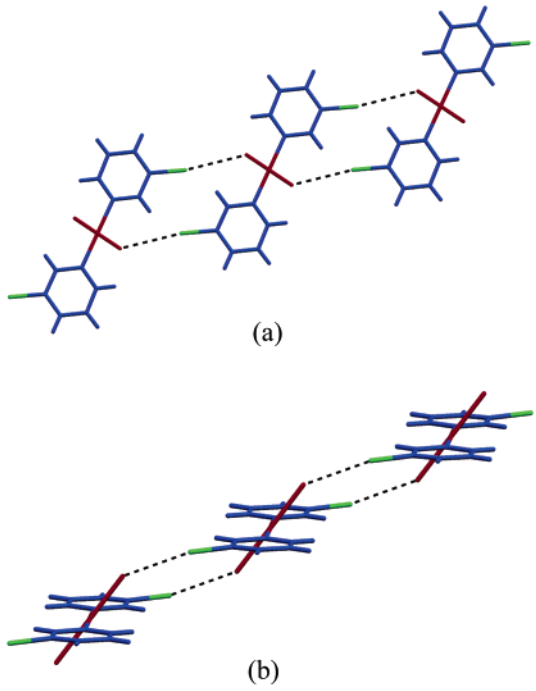

Figure 3. Views of **3b** showing the tape network propagated via Pt−Cl···Br−C interactions. Compound **8** is isostructural with **3b**, with the tape propagated through Pd−Cl···I−C interactions. Colors are as in Figure 2.

of these interactions appears to directly reinforce the Pt−Cl···Cl−C interactions (Figure 13, vide infra).

In structures **3b** and **8** the halogen−halogen interactions show geometries that are qualitatively analogous to those in **2** [(Pt)Cl···Br(C) 3.431(2) Å, Pt−Cl···Br 126.5(1)°, C−Br···Cl 166.6(2)° for **3b**; (Pd)Cl···I(C) 3.389(1) Å, Pd−Cl···I 121.98(3)°, C−I···Cl 169.2(1)° for **8**]. The ribbons aggregate in sheets via secondary C−H···Cl−M interactions [(C)H···Cl(Pt) 2.693 Å, C−H···Cl 166.0°, Pt−Cl···H 108.3° for **3b**; (C)H···Cl(Pd) 2.848 Å, C−H···Cl 171.0°, Pt−Cl···H 104.2° for **8**], and these sheets stack along the minor axis (*c*) of the unit cell via further C−H···Cl−M interactions [(C)H···Cl(Pt) 2.871, (2.996) Å,

Table 2. Halogen−Halogen Interaction Geometries

	interaction	(M)Cl···X(C) distance, Å	M−Cl···X angle, deg	C−X···Cl angle, deg	($r_{Cl} + r_X$), Å[a]	R_{ClX}[a]
2	Pt−Cl···Cl−C	3.443(1)	92.69(3)	155.9(1)	3.50	0.98
3a	Pt−Cl···Br−C	3.429(3)	137.1(1)	165.7(3)	3.60	0.95
		3.339(3)	126.1(1)	172.0(3)	3.60	0.93
3b	Pt−Cl···Br−C	3.431(2)	126.5(1)	166.6(2)	3.60	0.95
4	Pt−Cl···I−C	3.306(2)	131.7(1)	170.0(2)	3.71	0.89
6	Pd−Cl···Cl−C	3.596(4)	121.1(1)	159.3(3)	3.50	1.03
7	Pd−Cl···Br−C	3.534(1)	121.69(3)	158.2(1)	3.60	0.98
8	Pd−Cl···I−C	3.389(1)	121.98(3)	169.2(1)	3.71	0.91

[a] $R_{ClX} = d(Cl\cdots X)/r_{Cl} + r_X$, where r_{Cl} and r_X are, respectively, the van der Waals radii[26] of Cl and X (following the definition of Lommerse et al.[5]).

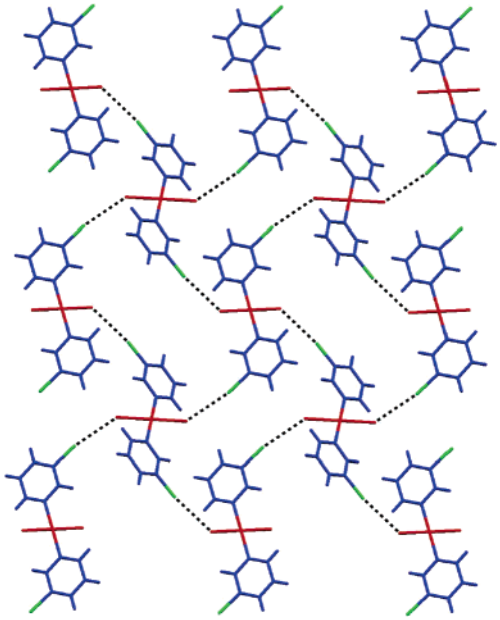

Figure 4. View of **3a** showing the 2D network propagated via Pt−Cl···Br−C interactions. Colors are as in Figure 2.

C−H···Cl 136.2° (138.6°), Pt−Cl···H 101.0° (100.0°) for **3b**; (C)H···Cl(Pd) 2.772, 2.860 Å, C−H···Cl 140.9, 138.0°, Pt−Cl···H 104.3, 104.6° for **8**] and via offset stacking interactions of *translationally* related halopyridine rings (Table 2 and Figure 12b, vide infra).

Layer Structures of *trans*-[$PtCl_2(NC_5H_4Br\text{-}3)_2$] (3a), *trans*-[$PdCl_2(NC_5H_4Cl\text{-}3)_2$] (6), and *trans*-[$PdCl_2(NC_5H_4Br\text{-}3)_2$] (7). The structures **6**, **7**, and polymorph **3a** contain 2D motifs propagated via M−Cl···X−C interactions (**6**, X = Cl, M = Pd; **7**, X = Br, M = Pd; **3a**, X = Br, M = Pt) through which each molecule interacts with four neighbors, as shown in Figures 4 and 5. Viewing each molecule as a 4-connected node, the 2D network is of (4,4) topology. Again, in all three structures these are the only halogen−halogen interactions present. Compounds **6** and **7** are isostructural, as is evident from unit cell parameters. The structure of **3a** is quite similar to the other pair, indeed topologically identical, but has a lower space group symmetry, which results in the presence of two independent molecules for **3a**.[25] A more undulating layer arrangement is found in **3a**, where the angle between the pyridine ring planes of neighboring molecules reaches 59.8°, while the corresponding angle in **6**

(25) Although $Z' = 1$ for **3a**, there the asymmetric unit comprises two independent half molecules, each situated at an inversion centre. For all other structures reported herein, $Z' = 0.5$.

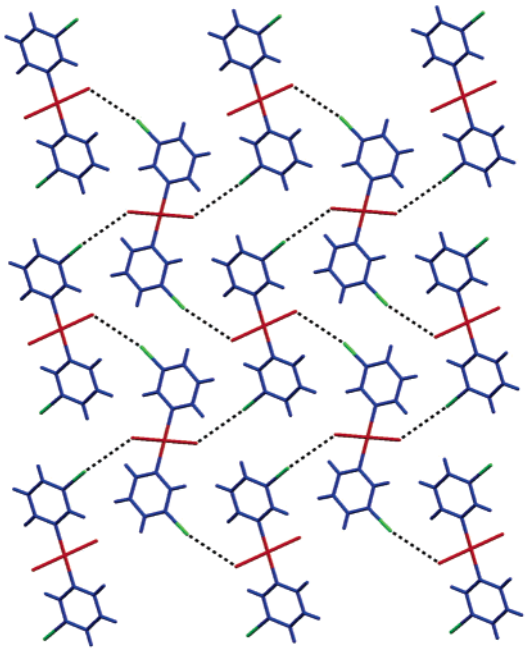

Figure 5. View of **7** showing the 2D network propagated via Pd−Cl···Br−C interactions. Compound **6** is isostructural with **7**, but the network is propagated through Pd−Cl···Cl−C interactions. Colors are as in Figure 2.

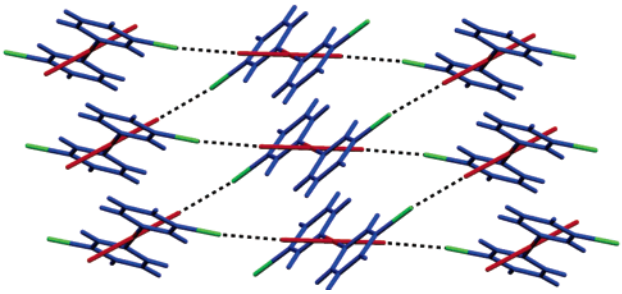

Figure 6. View of **4** showing the 2D network propagated via Pt−Cl···I−C interactions. Colors are as in Figure 2.

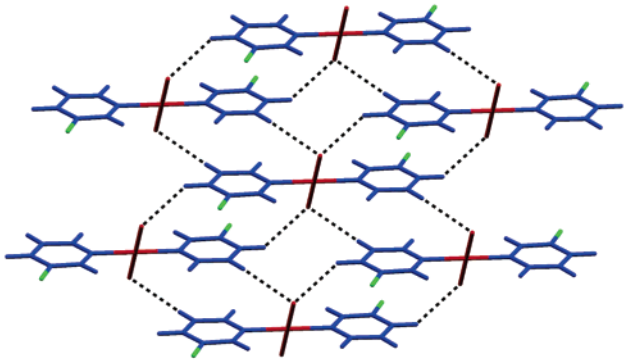

Figure 7. View of **1** showing C−H···Cl−Pt hydrogen bonds (dashed lines) and halopyridine ring stacking. Colors are as in Figure 2.

and **7** is 13.6° and 13.5°, respectively. The difference is associated with a slightly different molecular conformation adopted by **3a** [C−N−M−Cl torsion angle 133.9°, 132.1° (**3a**), 121.1° (**6**), 121.2° (**7**)] and shorter halogen−halogen interactions for **3a** than for **6** and **7** [(Pt)Cl···Br(C) 3.339(3), 3.429(3) Å, Pt−Cl···Br 126.1(1)°, 137.1(1)°, C−Br···Cl 172.0(3)°, 165.7-(3)° for **3a**; (Pd)Cl···Cl(C) 3.596(4) Å, Pd−Cl···Cl 121.1(1)°,

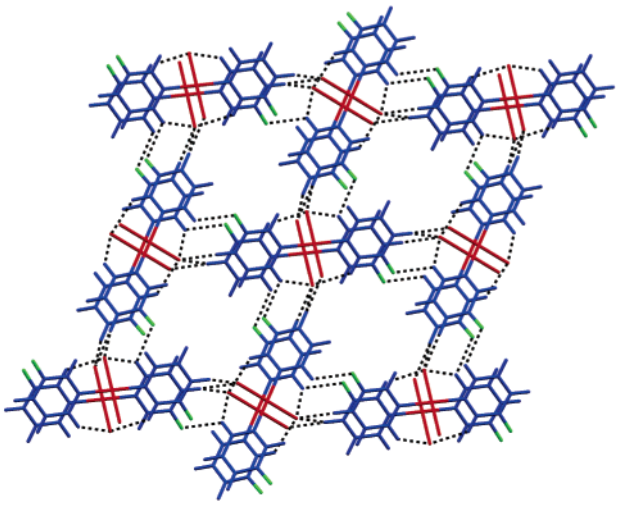

Figure 8. View of **5**·MeOH approximately along the *a*-axis showing channel structure. Disordered methanol molecules, which lie in the channels, are not shown. Colors are as in Figure 2.

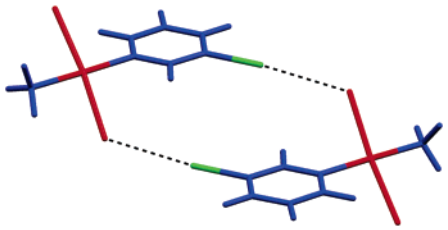

Figure 9. DFT optimized geometry of the dimer of *trans*-[$PdCl_2(NH_3)(NC_5H_4I)$]. The bromo- and chloropyridine analogues adopt very similar geometries. Colors are as in Figure 2.

C−Cl···Cl 159.3(3)° for **6**; (Pd)Cl···Br(C) 3.534(1) Å, Pd−Cl···Br 121.69(3)°, C−Br···Cl 158.2(1)° for **7**]. In these three structures, the layers are linked via offset stacking interactions of *translationally* related halopyridine rings (Table 2, vide supra) and C−H···Cl−M interactions [(C)H···Cl(Pt) 2.683, 2.784 Å, C−H···Cl 139.2°, 133.9°, Pt−Cl···H = 96.7, 96.3° for **3a**; (C)H···Cl(Pd) 2.783, 2.788 Å, C−H···Cl 134.3°, 136.2°, Pd−Cl···H = 104.6°, 103.9° for **6**; (C)H···Cl(Pd) 2.793, 2.807 Å, C−H···Cl 135.1°, 135.3°, Pd−Cl···H = 104.9°, 104.5° for **7**].

Layer Structure of *trans*-[$PtCl_2(NC_5H_4I\text{-}3)_2$] (4). Compound **4** adopts a layer structure in which each molecule is linked to four neighbors via Pt−Cl···I−C interactions [(Pt)Cl···I(C) 3.306(2) Å, Pt−Cl···I 131.7(1)°, C−I···Cl 170.0(2)°] to give a 2D network of (4,4) topology. However, the relative orientation differs from that of **3a**, **6**, and **7** in that offset stacking interactions of *translationally* related halopyridine rings occurs between neighboring molecules *within* the layer rather than between layers (Figure 6; Table 2, vide supra). As in the previous structures, the stacking interactions are supported by C−H···Cl−Pt hydrogen bonds [(C)H···Cl(Pt) 2.701 Å, C−H···Cl 147.7°, Pt−Cl···H = 91.0°]. Stacking of the layers is assisted by further C−H···Cl−Pt hydrogen bonds [(C)H···Cl(Pt) 2.745 Å, C−H···Cl 168.7°, Pt−Cl···H 140.0°].

Structures of *trans*-[$PtCl_2(NC_5H_4F\text{-}3)_2$] (1) and *trans*-[$PdCl_2(NC_5H_4F\text{-}3)_2$]·MeOH (5·MeOH). In the structures of **1** and **5**·MeOH halogen−halogen interactions are absent. In **1** molecules are linked primarily through C−H···Cl−Pt hydrogen bonds [(C)H···Cl(Pt) 2.777, 2.784, 2.785 Å, C−H···Cl 140.6°,

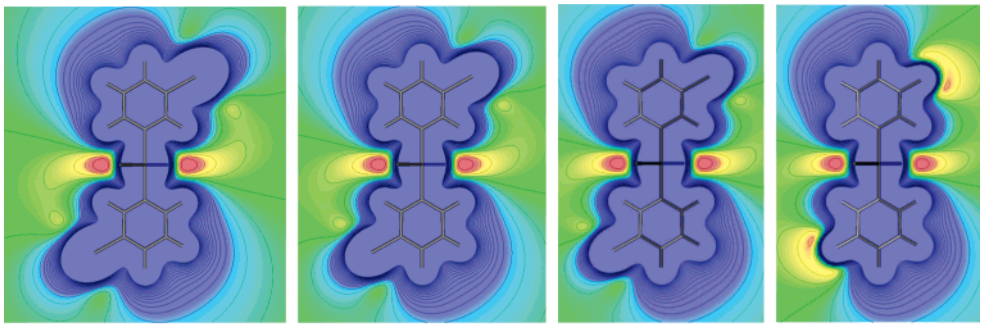

Figure 10. Calculated electrostatic potential for *trans*-[$PdCl_2(NC_5H_4X\text{-}3)_2$], (a) X = I, (b) Br, (c) Cl, (d) F, shown in the plane of the pyridine rings. (Note that the chloride ligands do not lie in this plane. Thus the negative potential associated with these ligands is substantially greater than appears in these figures; e.g. see ref 8a.) Contour interval 2.5 kcal/mol. Colors: blue (most positive), red (most negative).

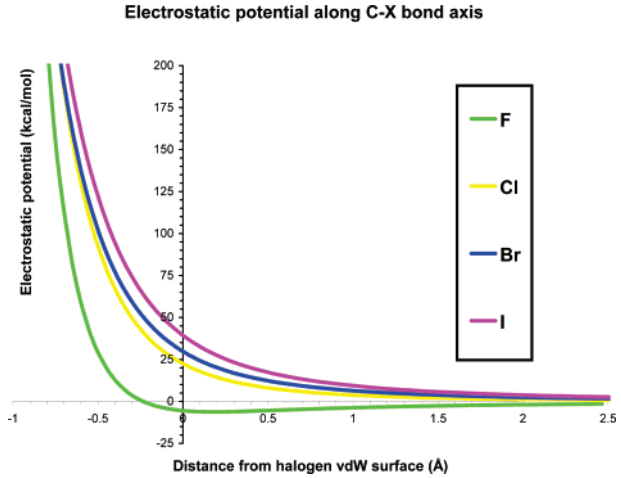

Figure 11. Calculated electrostatic potential for *trans*-[$PdCl_2(NC_5H_4X\text{-}3)_2$] (X = F, Cl, Br, and I, as indicated) plotted along the C−X bond axis. In each case zero represents a distance from the halogen nuclear position corresponding to the van der Waals radius[26] of that halogen.

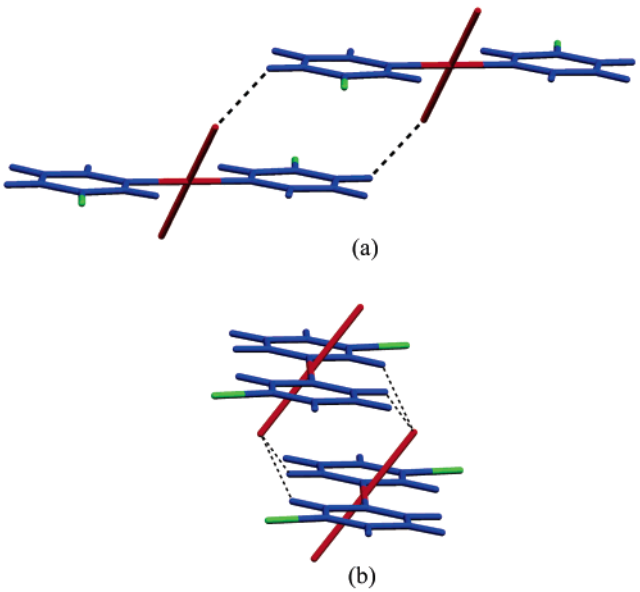

Figure 12. Offset $\pi-\pi$ stacking interactions found between 3-halopyridine rings: (a) centrosymmetrically stacked; (b) translationally stacked. Colors are as in Figure 2.

131.1°, 128.9°, Pt−Cl···H 104.2°, 104.3°, 118.7°] and via offset stacking interactions involving *centrosymmetrically* related halopyridine rings of neighboring molecules (Figure 7; Table 2, vide supra). Long C−H···F−C contacts (2.66 Å) are also noted.

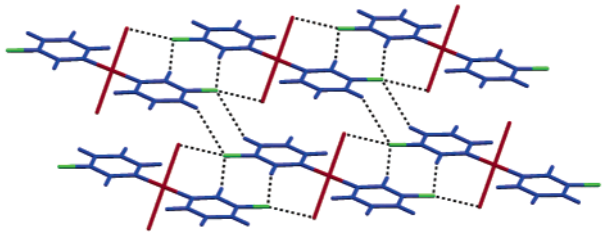

Figure 13. Role of C−H···Cl−C interactions in the cross-linking of Pt−Cl···Cl−C bonded tapes in **2**. Pt−Cl···Cl−C interactions are also shown. Colors are as in Figure 2.

In **5**·MeOH the [$PdCl_2(NC_5H_4F\text{-}3)_2$] molecules assemble into a layer arrangement via C−H···Cl−Pd hydrogen bonds [(C)H···Cl(Pd) 2.864 Å, C−H···Cl 131.9°, Pd−Cl···H 105°] and weak C−H···F−C interactions (2.56 Å) (Figure 8). The sheets stack via offset stacking interactions involving *translationally* related halopyridine rings of neighboring molecules (Table 2, vide supra) coupled with further C−H···Cl−Pd hydrogen bonds [(C)H···Cl(Pd) 2.695, 2.770 Å, C−H···Cl 139.9°, 135.2°, Pd−Cl···H 152.4°, 102.4°]. The resulting structure has channels running parallel to the *a*-axis which are occupied by disordered methanol molecules based upon best efforts to model the solvate crystallographically.

Theoretical Calculations on Dimers of the Model Complexes *trans*-[$PdCl_2(NH_3)(NC_5H_4X\text{-}3)$] (X = F, Cl, Br, I). To further explore the fact that M−Cl···X−C interactions are found to be prevalent in the structures of *trans*-[$MCl_2(NC_5H_4X\text{-}3)_2$] (X = I, Br, Cl) but absent in *trans*-[$MCl_2(NC_5H_4F\text{-}3)_2$], we have undertaken a series of DFT calculations to examine the optimized geometries of putative dimers of the model complexes *trans*-[$PdCl_2(NH_3)(NC_5H_4X\text{-}3)$] (X = I, Br, Cl, F). The starting dimer geometry used for subsequent optimizations was based upon that observed between neighboring molecules in the tape structure of **8** (and similar to that found in **2** and **3b**). Optimized dimer geometries (Figure 9) for the iodo, bromo, and chloro derivatives showed good agreement with the observed geometries within the tape structures of **8**, **3b**, and **2**, respectively, with Pd−Cl···X−C interactions having approximately linear C−X···Cl angles and Pd−Cl···X angles in the range 121−128°. Average (Pd)Cl···X(C) distances were calculated as 3.390 Å (X = I), 3.479 Å (X = Br), and 3.429 Å (X = Cl), all within the sum of van der Waals radii for the pair of halogens involved. By contrast, the *trans*-[$PdCl_2(NH_3)(NC_5H_4F)$] dimer is

much expanded from its starting geometry, with the shortest (Pd)Cl···F(C) separation being 4.622 Å, consistent with the absence of such interactions in structures **1** and **5**·MeOH.

Electrostatic Potential Calculations on the Complexes *trans*-[$PdCl_2(NC_5H_4X\text{-}3)_2$] (X = F, Cl, Br, I). The electrostatic potential distribution was calculated for the series of compounds *trans*-[$PdCl_2(NC_5H_4X\text{-}3)_2$] (X = F, Cl, Br, I) using averaged geometries close to those experimentally observed, differing only in the C−X bond lengths between the set of four compounds.

Clearly evident is the positive potential associated with the organic halogens (X ≠ F) (Figure 10). The potential decreases in the sequence I > Br > Cl and becomes negative for fluorine, as quantified along the direction of the C−X bond axis in Figure 11. This is consistent with the premise that placing the organic halogen as a substituent on a coordinated pyridine ring provides an enhancement of the electrophilicity of organic halogens (Scheme 3) and highly pertinent to their propensity to form M−Cl···X−C (X ≠ F) halogen bonds in the crystal structures of the compounds reported herein.

Discussion

Supramolecular assembly typically involves a number of different types of noncovalent interactions that facilitate molecular recognition and the assembly of supermolecules or extended supramolecular structures. Discovering new interactions and assessing the reliability of interactions and motifs in terms of both geometric reproducibility and likelihood of formation is a vital part of developing successful supramolecular synthetic strategies. A successful strategy often takes advantage of a correct assessment of the hierarchy of intermolecular forces that dictate a given assembly. This concept has been articulated in the context of hydrogen bonds by Etter[27] and recently applied to some highly successful supramolecular syntheses employing *iso*-nicotinamide by Aakeröy and coworkers.[28] In the present study four classes of interactions have been identified, namely, M−Cl···X−C interactions, offset π-stacking interactions between aromatic rings, C−H···Cl−M hydrogen bonds, and C−H···X−C interactions. Their role in the supramolecular assembly of the family of molecules is discussed below.

Halogen Bonds. The most significant finding of this study is that for all compounds, except the fluoropyridine systems in **1** and **5**, their crystal structures contain networks within which molecules are linked via M−Cl···X−C interactions. The geometries of these interactions are reliable and consistent (Table 2). Angles approaching linearity are observed at the organic halide (C−X···Cl), while much smaller obtuse angles are found at the inorganic halide (M−Cl···X).[29] (M)Cl···X(C) distances are typically shorter than the sum of van der Waals radii for the pair of halogens involved, i.e., $R_{ClX} < 1.0$.

These observations are strongly indicative that the inorganic and organic halogens are serving different roles in the M−Cl···X−C interactions, the former as a Lewis base and the latter as a Lewis acid. The attractive nature of the M−Cl···X−C interactions (X ≠ F) can be assumed from the fact that the electrostatic term will be attractive.[5] This is evident from the alignment of the region of electrostatic potential minimum of the M−Cl group with the electropositive axial region of the C−X groups. A repulsive electrostatic contribution to putative M−Cl···F−C interactions would result in a net repulsive interaction and presumably is significant in accounting for the absence of such interactions in the crystal structures of **1** and **5**·MeOH.

This chemical description of the M−Cl···X−C interactions is reinforced by the fact that normalized Cl···X distances, R_{ClX}, decrease and the directionality of the interaction (linearity of C−X···Cl) increases with change of pyridine substituent X from Cl to Br to I, consistent with the increased ability of the C−X functional group to act as Lewis acid along the series of halogens (Cl < Br < I). This decrease in Lewis acidity (electrophilicity) arises from the diminishing positive electrostatic potential associated with the organic halogen (I > Br > Cl; Figure 10a−c, Figure 11) and because of the analogous progressive stabilization of the C−X σ^* acceptor orbital (Scheme 1, **I**). The trend in R_{ClX} values with X is also consistent with our earlier observations involving charge-assisted M−Cl···X−C interactions.[14a] Thus, M−Cl···X−C interactions can be viewed as halogen bonds analogous to N···X−C, O···X−C, and similar interactions and most probably stabilized by similar attractive contributions (electrostatic and dispersion, with small charge transfer and polarization components) coupled with decreased repulsion for approaches along the C−X bond axis.[5] A full theoretical investigation of the nature of these interactions is planned.

In this series of structures all halogens except fluorine participate in M−Cl···X−C halogen bonds. Furthermore, there are no other halogen−halogen short contacts, though weak hydrogen bonds of the type C−H···Cl−M, and in some cases C−H···X−C, are observed (vide infra). This suggests that M−Cl···X−C halogen bonds can provide an effective synthon for supramolecular synthesis. Indeed, to use the terminology of Aakeröy,[28] the syntheses of **2**, **3a**, **3b**, **4**, **6**, **7**, and **8** provide a 100% supramolecular yield based upon the M−Cl···X−C synthon (X = I, Br, Cl), while structures of **1** and **5** (as **5**·MeOH) represent a 0% supramolecular yield for the putative M−Cl···F−C synthon. These synthons clearly merit further investigation in the face of other competing synthons since even some of the most widely used hydrogen-bonding synthons such as carboxylic acid or amide dimers have quite low success rates (33 and 8%, respectively) when considered in all crystal structures, while these can rise to above 90% through choice of appropriate molecular building blocks.[30] However, their success in these structures involving neutral building blocks coupled with earlier evidence from analogous charge-assisted interactions[14,31] suggests that M−Cl···X−C halogen bond synthons could provide a highly valuable tool for supramolecular assembly, particularly given the widespread accessibility of halogenated inorganic and organic compounds.

(26) Bondi, A. J. *J. Phys. Chem.* **1964**, *68*, 441.
(27) Etter, M. C. *Acc. Chem. Res.* **1990**, *23*, 120.
(28) Aakeröy, C. B.; Beatty, A. M.; Helfrich, B. A. *J. Am. Chem. Soc.* **2002**, *124*, 14425.
(29) This resembles the situation reported by Desiraju for C−X···X′−C interactions in which X ≠ X′, wherein typically a near linear angle is observed at the heavier (more electrophilic) halogen and a markedly bent angle at the lighter (more nucleophilic) halogen. See: Pedireddi, V. R.; Reddy, D. S.; Goud, B. S.; Craig, D. C.; Rae, A. D.; Desiraju, G. R. *J. Chem. Soc., Perkin Trans. 2* **1994**, 2353.
(30) Allen, F. H.; Motherwell, W. D. S.; Raithby, P. R.; Shields, G. R.; Taylor, R. *New J. Chem.* **1999**, *23*, 25.
(31) Jones has reported a number of examples of C−X···X$^-$ interactions: (a) Freytag, M.; Jones, P. G. Ahrens, B.; Fischer, A. K. *New J. Chem.* **1999**, *23*, 1137. (b) Jones, P. G.; Vancea, F. *CrystEngComm* **2003**, 303.

Table 3. Inter-ring Geometries for Stacking Interactions

	interplanar distance (Å)	centroid-to-centroid istance (Å)	offset angle (deg)[a]	type of stacking interaction[b]
1	3.329	3.708	26.1	C
	3.393	3.632	20.9	C
2	3.362	4.716	44.5	C
	3.099	4.799	49.8	C
3a	3.439	3.979	30.2	T
	3.449	3.979	29.9	T
3b	3.441	3.967	29.8	T
4	3.419	4.203	35.5	T
5	3.411	3.848	27.6	T
6	3.430	3.911	28.7	T
7	3.457	3.950	28.9	T
8	3.477	4.150	33.1	T

[a] Angle between the centroid−centroid vector and the normal to one of the pyridine ring planes (see ref 12). [b] C = centrosymmetrically related rings (see Figure 12b); T = translationally related rings (see Figure 12a).

Stacking Interactions. Aromatic−aromatic or $\pi-\pi$ stacking interactions are well-known across the spectrum of molecules containing aromatic rings. Such interactions can be rationalized in terms of a set of rules proposed by Hunter and Sanders in which the σ and π framework electrons are treated separately wherein net attractive interactions arise where $\sigma-\pi$ attractions overcome $\pi-\pi$ repulsions.[32] Janiak has examined the stacking interactions of pyridine and related ligands[12] which are appreciably less electron-rich than the prototypical benzene ring and have a greater tendency to form offset parallel stacking interactions which emphasize the $\sigma-\pi$ attraction and benefit from the electrostatic attraction between the permanent local dipoles associated with such ligands. In all the structures described in the present study, offset parallel stacking interactions are present. Two distinct stacking geometries are found, in which the stacked halopyridine rings from neighboring molecules are related centrosymmetrically (Figure 12a) or by a simple translation[33] (Figure 12b). The former is noted by Janiak to be a common configuration between pyridine ligands,[12] although the latter is more prevalent in the *trans*-$[PdCl_2(NC_5H_4X\text{-}3)_2]$ systems, occurring exclusively in compounds **3**−**8**. Geometries of the stacking interactions conform well to typical values established by Janiak, with interplanar separations all close to 3.4 Å and offset angles of 20−50° (Table 3). The prevalence of the translationally stacked interaction can perhaps be attributed to its augmentation by a set of up to four C−H···Cl−M hydrogen bonds (Figure 12b) available for this family of compounds.

C−H···Cl−M and C−H···X−C Interactions. That C−H···Cl−M interactions are viable hydrogen bonds, weaker, but with similar though less sharply defined angular characteristics as their stronger N−H···Cl−M and O−H···Cl−M analogues, has been well established by a number of detailed studies.[8a,34,35] Thus, the occurrence of these hydrogen bonds throughout these structures should be of no surprise. However, while the M−Cl···H(C) acceptor angles lie overwhelmingly within the preferred angular range (viz., 100−120°), C−H···Cl(M) angles are substantially displaced from linearity (viz., 125−140°) in all but three of the 21 interactions observed. This suggests that C−H···Cl−M hydrogen bonds, while important due to their shear numbers, probably play a supporting role in the overall hierarchy of interactions given their readiness to distort from optimum geometries.

We finally turn to what is undoubtedly the weakest of the four classes of noncovalent interactions identified in these crystal structures, namely, the C−H···X−C interactions. We have previously shown that C−H···X−C interactions show all the geometric hallmarks of weak hydrogen bonds in terms of both C−H···X(C) and C−Cl···H(C) angles,[8a] an assertion supported in terms of C−H···X(C) angle distribution by the earlier study of Seddon and Aakeröy,[34] whereas Thallypally and Nangia concluded[35] that C−H···X−C close contacts should generally be considered as van der Waals interactions. In the present family of structures there is some suggestion that dimerization of neighboring molecules in certain directions is supported by a cyclic $R_2^2(8)$ motif, most prominently illustrated in the structure of **2** (Figure 13). Here geometries of the two independent interactions are (C)H···X(C) 2.759, 2.894 Å; C−H···X 163.9°, 132.1°; and C−Cl···H 111.8°, 118.4°. The former, which supports the Pt−Cl···Cl−C interaction, has a roughly linear geometry, makes an optimum angle at the chlorine acceptor, and exhibits a (C)H···X(C) distance some 0.19 Å shorter than the sum of hydrogen and chlorine van der Waals radii. Tapes propagated by this cyclic $R_2^2(8)$ motif involving either C−H···Cl−C or C−H···Br−C hydrogen bonds have also been reported by Palmore and co-workers.[36] Very recently Desiraju and Howard have reignited the debate over the potential importance of these types of weak interactions in crystal engineering with a study of intramolecular O−H···Cl−C interactions.[37]

Polymorphism. Only one of the eight compounds studied (*trans*-$[PtCl_2(NC_5H_4Br\text{-}3)_2]$ (**3**)) was confirmed to be polymorphic. However, it is likely that polymorphism is more prevalent at least in the nonfluorinated compounds given their similarity in molecular shape and the fact that five structural arrangements have been observed, viz., compound **2**, isostructural compounds **3b** and **8**, compound **3a**, isostructuctural compounds **6** and **7**, and compound **4**. All molecular crystal structure arrangements involve a compromise between efficient molecular packing[38] and maximizing attractive over repulsive interactions. Thus, one might anticipate that further exploration of crystallization conditions may lead to alternative polymorphs for some of these compounds that are consistent with the structural arrangements already observed within this family.

Conclusions

This systematic study of the family of compounds *trans*-$[MCl_2(NC_5H_4X\text{-}3)_2]$ (M = Pt, Pd; X = I, Br, Cl, F) demonstrates the importance of M−Cl···X−C interactions where X ≠ F. All halogens participate in these interactions and in no other halogen−halogen interactions, giving rise to 1D molecular tapes or 2D layer structures. The roles of the inorganic halogen

(32) (a) Hunter, C. A.; Sanders, J. K. M. *J. Am. Chem. Soc.* **1990**, *112*, 5525. (b) Hunter, C. A. *Chem. Soc. Rev.* **1994**, *23*, 101.
(33) Note that the translation between rings is not normal to the ring planes but rather along the centroid−centroid vector, which is inclined to the normal of ring plane(s) at the offset angle (see Table 2).
(34) Aakeröy, C. B.; Evans, T. A.; Seddon, K. R.; Pálinkó, I. *New J. Chem.* **1999**, *23*, 145.
(35) Thallypally, P. K.; Nangia, A. *CrystEngComm* **2001**, *3*, 114
(36) (a) McBride, M. T.; Luo, T.-J. M.; Palmore, G. T. *Cryst. Growth Des.* **2001**, *1*, 39. (b) Luo, T.-J. M.; Palmore, G. T. *Cryst. Growth Des.* **2002**, *2*, 337.
(37) Banerjee, R.; Desiraju, G. R.; Mondal, R.; Howard, J. A. K. *Chem. Eur. J.* **2004**, *10*, 3373.
(38) (a) Kitaigorodskii, A. I. *Molecular Crystals and Molecules*; Academic Press: New York, 1973. (b) Pidcock, E.; Motherwell, W. D. S. *Chem. Commun.* **2003**, 3028.

(M−Cl) and the organic halogen (C−X) are distinct and different, as evidenced by the C−X···Cl and M−Cl···X angles, which consistently approach linearity at the organic halogen while being markedly angular (ca. 120−130°) at the inorganic chloride. The observed geometries are supported by DFT calculations using model dimers and suggest an attractive M−Cl···X−C interaction within which the organic and inorganic halogens function as electrophile and nucleophile, respectively. This supposition is reinforced by the reduction in interaction distance (R_{ClX}) as the pyridine substituent X descends the halogen group and by the complete absence of M−Cl···F−C interactions. Thus, M−Cl···X−C interactions should clearly be classified as halogen bonds alongside N···X−C, O···X−C, and other similar cases. The potential efficacy of M−Cl···X−C halogen bonds is highlighted by their consistent presence and geometry in the presence of three other identified categories of noncovalent interactions, namely, offset $\pi-\pi$ stacking, C−H···Cl−M hydrogen bonds, and in some cases C−H···X−C hydrogen bonds, which collectively contribute to the overall 3D structures observed.

Acknowledgment. L.B. and F.Z. are grateful to Harry Adams (Sheffield) for helpful discussions regarding the crystal structure determinations and the EPSRC (GR/R68733/01) for support of this work.

Supporting Information Available: X-ray crystallographic files in CIF format for compounds **1**−**8**. Experimental and calculated powder patterns for compounds **1**−**8**. DFT optimized geometries of dimers of *trans*-[$PdCl_2(NH_3)(NC_5H_4X$-3)] model complexes (X = I, Br, Cl, F). Geometries used in DFT calculations of electrostatic potentials of *trans*-[$PdCl_2$-$(NC_5H_4X$-3$)_2$] (X = I, Br, Cl, F). This material is available free of charge via the Internet at http://pubs.acs.org.

JA0435182